Ultrastructural identification of uncoated caveolin-independent early endocytic vehicles

Matthew Kirkham,[1,2,3] Akikazu Fujita,[1,2,3] Rahul Chadda,[6] Susan J. Nixon,[1,2,3] Teymuras V. Kurzchalia,[4] Deepak K. Sharma,[5] Richard E. Pagano,[5] John F. Hancock,[1] Satyajit Mayor,[6] and Robert G. Parton[1,2,3]

[1]Institute for Molecular Bioscience, [2]Centre for Microscopy and Microanalysis, and [3]School of Biomedical Sciences, University of Queensland, Queensland 4072, Australia
[4]Max Planck Institute for Molecular Cell Biology and Genetics, Dresden D-01307, Germany
[5]Department of Biochemistry and Molecular Biology, Mayo Clinic and Foundation, Rochester, MN 55905
[6]National Centre for Biological Sciences, Bangalore, 560 065, India

Using quantitative light microscopy and a modified immunoelectron microscopic technique, we have characterized the entry pathway of the cholera toxin binding subunit (CTB) in primary embryonic fibroblasts. CTB trafficking to the Golgi complex was identical in caveolin-1null (Cav1−/−) mouse embryonic fibroblasts (MEFs) and wild-type (WT) MEFs. CTB entry in the Cav1−/− MEFs was predominantly clathrin and dynamin independent but relatively cholesterol dependent. Immunoelectron microscopy was used to quantify budded and surface-connected caveolae and to identify noncaveolar endocytic vehicles. In WT MEFs, a small fraction of the total Cav1-positive structures were shown to bud from the plasma membrane (2% per minute), and budding increased upon okadaic acid or lactosyl ceramide treatment. However, the major carriers involved in initial entry of CTB were identified as uncoated tubular or ring-shaped structures. These carriers contained GPI-anchored proteins and fluid phase markers and represented the major vehicles mediating CTB uptake in both WT and caveolae-null cells.

Introduction

Endocytosis is a vital process required for many cellular processes including nutrient uptake, membrane recycling, and signal transduction. In comparison to the clathrin-mediated pathway, alternative nonclathrin endocytic pathways are poorly understood. However, evidence has accumulated over recent years for an internalization route involving a lipid-based sorting mechanism (Conner and Schmid, 2003; Parton and Richards, 2003). This pathway has been proposed to involve either caveolae, flask-shaped invaginations of the plasma membrane (PM) generated by the expression of caveolin-1 (Cav1), or other structures of undefined morphology but similar biochemical properties, which have been termed lipid rafts.

The nonenveloped virus simian virus 40 (SV40) and the bacterial protein cholera toxin (CT) have been extensively studied as potential markers of a nonclathrin pathway (Pelkmans et al., 2001; Parton and Richards, 2003). In fact, the pathways taken by these two agents show many similarities. Both pathways use the ganglioside GM1 as a surface receptor (Tsai et al., 2003); GM1 is enriched in caveolae (Parton, 1994) as well as in apparently featureless lipid raft domains, and both SV40 and CT are subsequently transported to the ER via a brefeldin A–sensitive trafficking pathway (Richards et al., 2002). The most compelling case for an entry pathway involving caveolae has come from the studies of SV40. SV40 shows a striking enrichment in caveolae as shown by immunoelectron microscopy (Stang et al., 1997) and light microscopy using a Cav1GFP fusion protein (Pelkmans et al., 2001). Interestingly, virus binding induces caveolae budding, suggesting that caveolae at steady state are relatively static surface features but budding can be regulated. This finding is consistent with independent FRAP studies of Cav1GFP (Thomsen et al., 2002) and earlier studies suggesting regulated internalization of caveolae in response to experimentally induced hyperphosphorylation using the phosphatase inhibitor okadaic acid (OA; Parton et al., 1994). Stimulation of caveolae budding by SV40 involves tyrosine phosphorylation and recruitment of actin and dynamin (Pelkmans et al., 2002). Similar characteristics of caveolae internalization have been shown in studies of the endocytosis of albumin (Minshall et al., 2000; Shajahan et al., 2004) and of specific

Correspondence to Robert G. Parton: R.Parton@imb.uq.edu.au

D.K. Sharma's present address is Photometrics, Roper Scientific, Tucson, AZ 85706.

Abbreviations used in this paper: AA, ascorbic acid; Cav1, caveolin-1; CT, cholera toxin; CTB, CT binding subunit; DN, dominant-negative; GEEC, GPI-AP–enriched early endosomal compartment; GPI-AP, GPI-anchored protein; LacCer, lactosyl ceramide; MEF, mouse embryonic fibroblast; OA, okadaic acid; PM, plasma membrane; SV40, simian virus 40; Tf, transferrin; TfR, transferrin receptor; WT, wild-type.

The online version of this article includes supplemental material.

The Journal of Cell Biology
http://www.jcb.org/cgi/doi/10.1083/jcb.200407078

Supplemental Material can be found at:
http://www.jcb.org/cgi/content/full/jcb.200407078/DC1

glycosphingolipids (Sharma et al., 2004). Intriguingly, the latter studies suggest that internalization of caveolae in this system is specifically stimulated by glycosphingolipids and by cholesterol as judged by light microscopy and loss of surface caveolae (Sharma et al., 2004). In addition, these studies have shown a role for PKC and Src kinases in caveolae internalization and showed activation of Src upon lipid addition (Sharma et al., 2004).

The involvement of caveolae in CT entry is less clear, and evidence for and against a role for caveolae has been generated in subsequent years. A series of elegant experiments showed that CT association with lipid rafts, as judged by sensitivity to cholesterol-disrupting agents and by generation of hybrid toxins with different lipid specificities, is crucial for CT toxicity (Orlandi and Fishman, 1998; Wolf et al., 1998). But are caveolae essential for CT endocytosis? Studies of CT endocytosis in cells that lack caveolae have yielded contradictory results. Although most studies have concluded that caveolae are not required for CT internalization occurring efficiently in cells lacking caveolae (Orlandi and Fishman, 1998; Torgersen et al., 2001; Nichols, 2002), a recent study concluded that CT entry did not occur in fibroblasts from mice lacking Cav1 and caveolae (Sotgia et al., 2002). Additionally, it has been shown that a significant amount of CT can enter various cell types through a clathrin-dependent pathway (Shogomori and Futerman, 2001; Torgersen et al., 2001; Nichols, 2002; Massol et al., 2004). The route by which CT enters the cell may also depend on the level of GM1 expression at the PM; when GM1 levels are increased, the pathway for CT uptake becomes more sensitive to cholesterol depletion, independently of Cav1 expression (Pang et al., 2004).

If caveolae are not essential for CT uptake, are there additional nonclathrin, noncaveolae lipid raft–dependent pathways CT can use? Other lipid raft markers such as GPI-anchored proteins (GPI-APs), originally thought to be endocytosed through a caveolae-dependent process (Anderson et al., 1992), have now been shown to enter the cell through a dynamin- and caveolae-independent, cdc42-dependent pinocytic pathway (Sabharanjak et al., 2002). Lipid raft–associated IL-2 has been shown to be internalized in a pathway independent of clathrin and caveolae but involving dynamin and RhoA (Lamaze et al., 2001).

Although evidence for a clathrin- and caveolae-independent pathway is accumulating, the lack of ultrastructural identification of the carriers involved in the initial entry step has hampered attempts to characterize the molecular machinery involved in this pathway. We have now used light microscopy and EM to examine CT entry in wild-type (WT) and Cav1-null primary fibroblasts. We show that CT can be endocytosed via three distinct pathways: clathrin coated pits, caveolae, and by a major clathrin- and caveolin-independent pathway, which we now characterize at the ultrastructural level for the first time.

Results

Development of an ultrastructural assay to quantitate caveolae budding

Our first aim was to examine the budding of individual caveolae at the ultrastructural level. One limiting factor in studying caveolae endocytosis has been the inability to distinguish individual internal caveolae from surface-connected structures, as particularly evident in certain cell types where surface-connected caveolae structures can appear in the perinuclear area of the cell (Parton et al., 2002). To discriminate between surface-connected and internal structures, we made use of the observation that the HRP reaction on an extracellular surface can be quenched by the use of the membrane-impermeable reducing agent ascorbic acid (AA; Stoorvogel et al., 1996). This method was optimized to discriminate between surface structures, even those with extremely narrow connections to the extracellular milieu, and internal budded structures (Fig. 1, protocol and validation; and Fig. S1, available at http://www.jcb.org/cgi/content/full/jcb.200407078/DC1). In addition, the method was modified to enable immunolabeling for caveolin to ensure that only bona fide caveolin-positive structures were recognized as budded caveolae. Labeled cell cultures were either processed for preparation of ultrathin sections or were prepared for visualization as whole-mount specimens using cells grown on grids.

To analyze caveolae budding, CT binding subunit (CTB) conjugated to HRP (CTBHRP) was bound to the surface at 4°C, and the cells were warmed for time periods between 15 s and 5 min. The DAB reaction was then performed on living cells in the presence of AA at 4°C to allow reaction product generation only in intracellular (budded) carriers. We focused on very early stages of internalization to identify the first endocytic carriers. At 4°C, no DAB-labeled profiles were observed, but after just 15 s of warming (adding warm media at time 0, and then replacing with ice-cold medium after 15 s) DAB-labeled profiles were evident (Fig. 1 and see Figs. 4 and 5). After the DAB reaction and paraformaldehyde fixation the cells were permeabilized and labeled for Cav1. The bulk of the Cav1 labeling at the periphery of the cell was observed on surface-connected CTBHRP-negative 60-nm-diam caveolae. However, careful examination of many cells revealed a small number of internal CTBHRP-positive budded caveolae after 15 s (Fig. 1) as well as vesicular structures of the size and morphology of clathrin coated vesicles and other tubular carriers (see Figs. 4 and 5). No DAB-labeled caveolae were observed in cells maintained at 4°C, showing that this small population of caveolae had budded during the short period of warming. Quantitation revealed that ~2% of the total pool of Cav1-positive caveolae were DAB positive, and thus detached from the cell surface after warming cells for 1 min (Fig. 1 E). Thus, caveolae can bud from the cell surface, but at steady state this represents a relatively small pool of caveolae. We also observed more complex structures labeled with internalized CTBHRP after 5 min of warming (Fig. 1 B). Some of these structures showed strong labeling of Cav1, and this often was associated with areas of distinct caveolar morphology (Fig. 1, A–C; and see Fig. 5, B and C). These structures are either caveosomes, to which CTBHRP has been delivered, or detached clusters of caveolae.

The use of this technique allowed us to identify budded Cav1-labeled structures for the first time. Previous studies have suggested that Cav1 can form endocytic carriers both by colocalization with endocytic markers and by biochemical assays (Introduction). These studies were not able to distinguish between

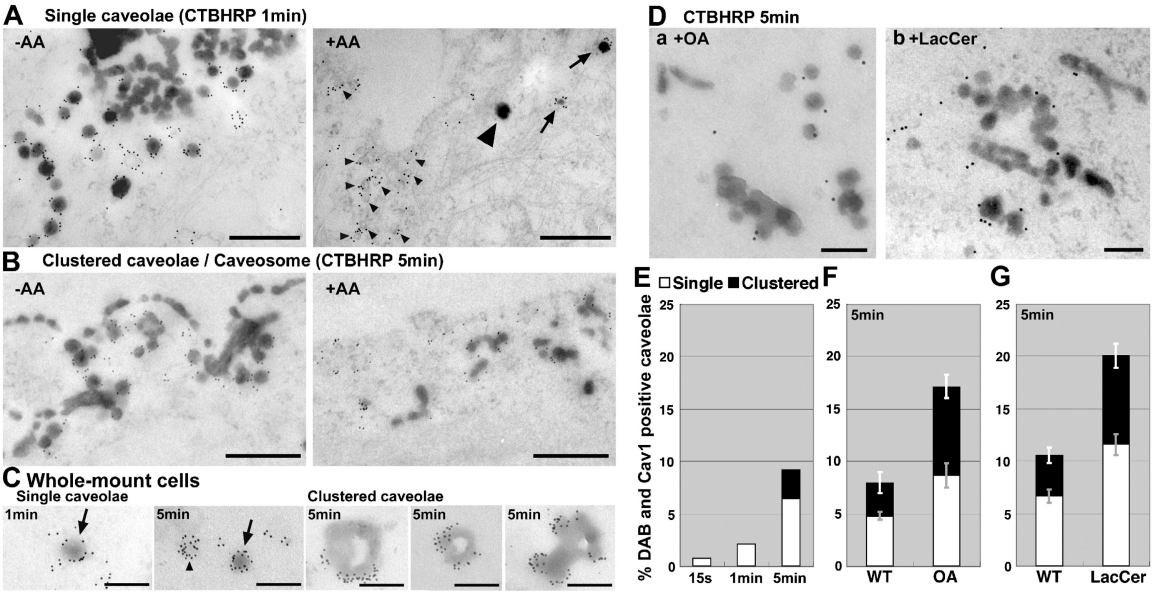

Figure 1. **Ultrastructural characterization of caveolae endocytosis.** (A and B) WT MEFs with bound CTBHRP were warmed for 1 (A) or 5 min (B). The DAB reaction was performed on ice in the presence (+AA) or absence (−AA) of AA, and then cells were processed for immunoelectron microscopy detection of Cav1. A and B are representative of areas enriched in caveolae. (A) DAB reaction product is present in a small subset of budded (nonsurface-connected) Cav1-positive caveolae (arrows) in cells treated with AA during the DAB reaction. A large number of caveolae were DAB negative and thus surface connected (small arrowheads). Putative budded clathrin vesicles were also observed (large arrowhead). (B) After 5 min of CTBHRP uptake, Cav1 also localized to DAB-positive internal structures (+AA), which had an irregular tubular morphology (defined operationally as clustered caveolae in E–G). (C) WT MEFs with CTBHRP internalized for either 1 or 5 min were treated with DAB in the presence of AA, labeled for Cav1, and processed for whole-mount visualization. Budded (DAB-positive) caveolae (arrow), surface-connected (DAB-negative) caveolae (arrowhead), and internal Cav1-positive larger structures were observed. (D) WT MEFs were treated as in A but warmed for 5 min in the presence or absence of either OA or LacCer before the DAB reaction in the presence of AA. (E–G) Quantitation of internal caveolae (single or clustered) as compared with the total number of caveolae present in the same area with increasing time of incubation at 37°C (E) or after 5 min at 37°C in the presence/absence of OA (F) or LacCer (G). Error bars indicate standard error. Bars: (A and B) 500 nm; (C and D) 200 nm.

individual caveolae that were surface connected, endocytic vesicle carriers, or those that were part of endosomal structures. The results presented here, identifying a small population of budded caveolae, are consistent with previous studies in which caveolae internalization appeared to be a relatively infrequent event but could be stimulated. In particular, the phosphatase inhibitor OA was shown to stimulate rapid internalization of caveolae as judged by both EM (in the absence of methods to immunolabel and identify budded caveolae) and using a biochemical method (Parton et al., 1994), and in other studies using SV40 as a marker in real-time light microscopic studies (Pelkmans et al., 2002). Additionally, it has been shown that caveolae internalization can be stimulated through the addition of glycosphingolipids such as lactosyl ceramide (LacCer) to the PM (Sharma et al., 2004). Therefore, we tested the effect of OA and LacCer in this system. Treatment with 1 μM OA during the 5-min warming step caused an increase in bona fide Cav1-positive CTBHRP-labeled structures from ~8% in control cells to 17% in OA-treated cells (Fig. 1, D–F). LacCer treatment caused a similar increase in internal Cav1-labeled structures from 11 to 20% (Fig. 1, D–G). In both cases, we observed an increase in both budded single caveolae and larger structures with caveolar morphology. In the absence of additional markers we cannot yet determine whether these structures are caveosomes (Pelkmans et al., 2001) or a group of caveolae that have budded as a unit from the PM (Parton et al., 1994). Nevertheless, these findings show that in this cell type, caveolae budding is infrequent but can be stimulated.

The results provide an explanation for numerous apparently contradictory observations in different systems (Severs, 1988; Parton and Richards, 2003; van Deurs et al., 2003). Although caveolae budding is infrequent, it can be stimulated by SV40 (and presumably physiological ligands), and may be more frequent in certain cell types, such as endothelial cells, than in other cells where caveolae have been suggested to be static (such as skeletal muscle [Kaisto et al., 1999] or adipocytes [Souto et al., 2003]). The methods described here provide sufficient sensitivity to identify and quantitate a small number of budded caveolae that may play an important role in cellular function.

CTB trafficking to the Golgi is identical in WT mouse embryonic fibroblasts (MEFs) and Cav1−/− MEFs

The aforementioned data show that in WT MEFs caveolae can play a role in CTB internalization. However, the question of whether or not caveolae are essential for CTB uptake remains controversial (Introduction). To address this question, we investigated the entry of CTB into WT or Cav1−/− MEFs by quantitative light and electron microscopy. Cav1−/− MEFs contained no morphologically identifiable caveolae (unpublished data). We first compared CTB uptake between the two cell cultures by confocal microscopy using conditions and reagents that were apparently identical to those used in previous studies (Sotgia et al., 2002). CTB binding to the surface was comparable between the two cell lines as judged by quantifica-

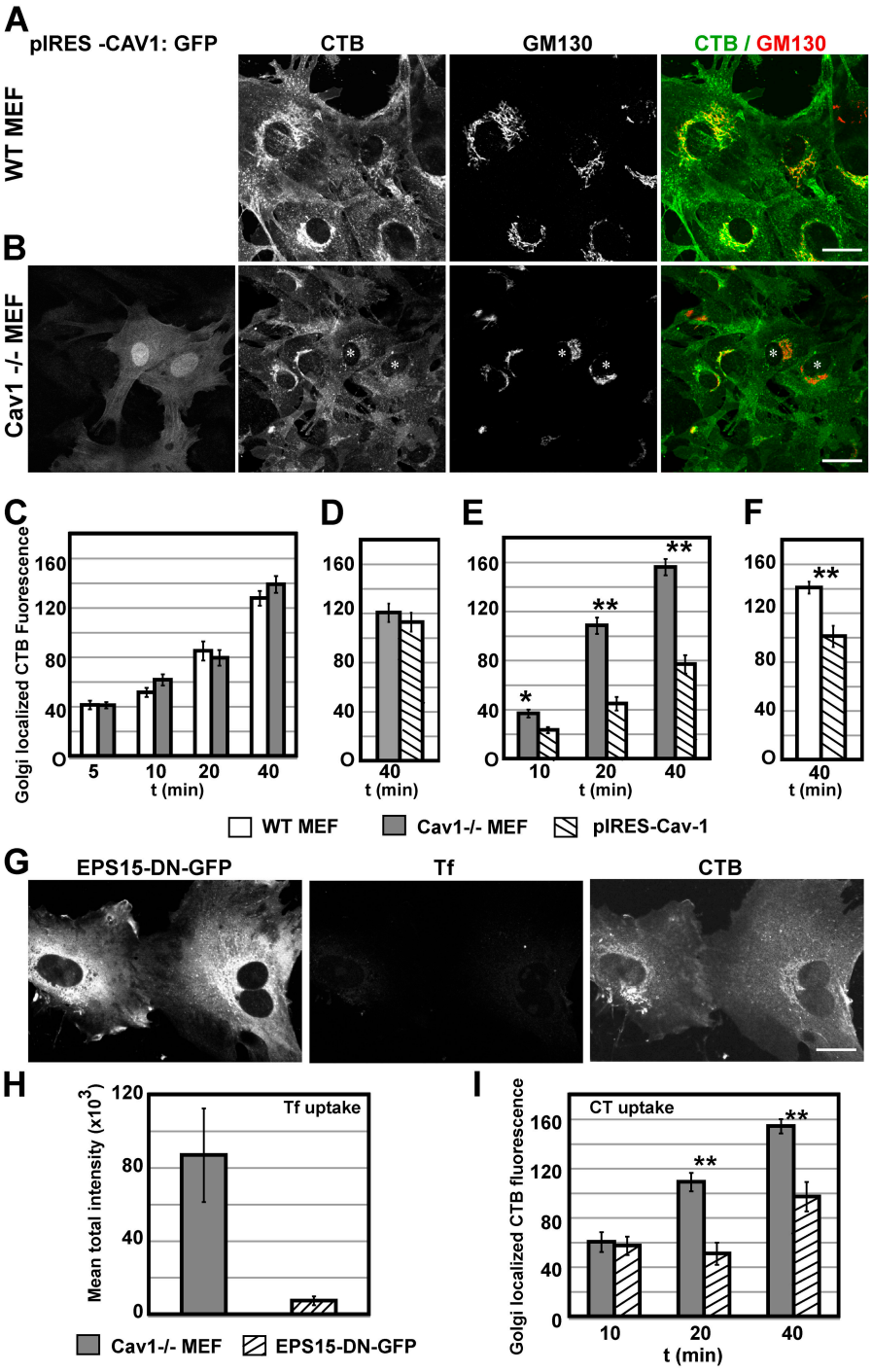

Figure 2. **Internalization of CTB by WT and Cav1−/− MEFs.** (A–F) CTB-FITC was internalized in WT MEFs (A and C) or Cav1−/− MEFs (C) at 37°C for various times, and then fixed and labeled for GM130 (A and C). The accumulation of CTB within the Golgi complex in both WT MEFs and Cav1−/− MEFs was quantified (C); no significant differences were seen. Bars indicate standard error. Cav1−/− MEFs were microinjected with pIRES-Cav-1 using standard conditions (D) and short expression conditions (B and E). (B) Injected cells (*) were marked by the production of cytosolic GFP coded for by the same message as untagged Cav1. CTB-Alexa Fluor 594 was internalized and CTB fluorescence intensity in the GM130-positive region was quantified (D–F). WT MEFs were microinjected with pIRES-Cav-1 using short expression conditions (F). Only short expression of Cav1 reduced CTB trafficking to the Golgi complex as compared with nonexpressing cells in both WT and Cav1−/− MEFs (D–F). (G) Cav1−/− MEFs were microinjected with vectors encoding for EPS15-DN-GFP and TfR for short expression. CTB-FITC was internalized simultaneously with Tf for 40 min. CTB-FITC was labeled with an anti-CT antibody and a secondary antibody conjugated to Alexa Fluor 660. In cells that were injected with EPS15-DN-GFP, Tf uptake was inhibited, but CTB still accumulated in a perinuclear compartment. (H) Cav1−/− MEFs were microinjected with vectors encoding TfR and either GFP or EPS15-DN-GFP (short expression), and then Tf uptake for 20 min was performed. Internal Tf was quantified in injected cells, and EPS15-DN-GFP inhibited Tf uptake by 90%. (I) Cav1−/− MEFs were microinjected with vectors encoding for EPS15-DN-GFP (short expression), and CTB-Alexa Fluor 594 was internalized for various times. Quantification of CTB accumulation in the GM130-positive Golgi complex revealed that EPS15-DN-GFP reduced CTB trafficking by only 40%. Bars indicate standard error; *, $P < 0.01$; **, $P < 0.001$. Bars, 25 μm.

tion of fluorescence intensity (unpublished data). CTB internalized in both WT and Cav1−/− MEFs occurred through qualitatively similar pathways with labeling of punctate peripheral structures followed by accumulation in a GM130-positive perinuclear compartment after 40 min (Fig. 2, A and B). The Golgi localization of CTB in Cav1−/− MEFs was confirmed by EM (unpublished data). Quantification of CTB accumulation in the Golgi complex (Fig. 2 C) showed that there were no significant differences between WT and Cav1−/− MEFs at any time point between 5 and 40 min. Similar results were obtained using a range of CTB concentrations from 0.05 to 1 μg/ml (unpublished data). These results show that CTB entry does not require caveolae. We investigated whether or not the two cell lines differed in their sensitivity to CT using a single cell toxicity assay (Massol et al., 2004). CT treatment (100 ng/ml for 2 h) caused cell rounding indicative of cAMP production in 38 ± 6% of WT MEFs and 40 ± 7% of Cav1−/− MEFs. No difference in sensitivity to CT between the two cell lines was observed at concentrations from 1 μg/ml to 1 ng/ml (unpublished data). Pretreatment of cells for 1 h with brefeldin A (5 μg/ml) greatly inhibited the alteration in the morphology of cells in the presence of CT (unpublished data). This finding supports the

light microscopic analysis of CTB trafficking to the Golgi complex in the two cell lines.

Although these findings are consistent with several studies showing that caveolae are not required for CTB entry (Orlandi and Fishman, 1998; Torgersen et al., 2001; Nichols, 2002), they are in apparent contradiction to the findings of Sotgia et al. (2002), who concluded that CTB uptake is dependent on Cav1 and caveolae within MEF-derived cell lines. In our hands, no conditions were found in which the WT and Cav1−/− MEFs differed in their handling of CTB. This was confirmed at the EM level. However, one possibly significant difference in the two studies is the use of immortalized cell lines of WT and Cav1−/− MEFs (Sotgia et al., 2002) rather than the primary cultures as used here. During cell immortalization, a clonal population of Cav1−/− MEF cells with distinct properties may have emerged. For example, Pang et al. (2004) reported variation in GM1 levels within tissue culture cell lines, and the subpopulation that contained low GM1 levels showed reduced CTB uptake independent of Cav1 expression.

In several studies, Cav1 expression has been shown to inhibit rather than stimulate clathrin-independent endocytosis (Minshall et al., 2000; Le et al., 2002; Sharma et al., 2004). Therefore, we transiently expressed Cav1 in Cav1−/− MEFs by microinjection of the cDNA. After an overnight incubation, CTB was added to the cells and accumulation in the Golgi complex was quantified in Cav1-expressing versus nonexpressing neighboring cells after a 40-min incubation. Cav1−/− MEFs transiently expressing Cav1 showed a slight reduction in levels of CTB in the Golgi, but this was not statistically significant when compared with the population of noninjected cells (Fig. 2 D). However, we noted a small number of highly expressing cells with a dramatic reduction in CTB accumulation (unpublished data). To investigate this further, WT and Cav1−/− MEFs were microinjected with a higher amount of the Cav1 cDNA and, after allowing expression for just 6 h, incubated with CTB. Short expression of Cav1 (Fig. 2, B, E, and F) but not short expression of GFP alone (not depicted) caused a significant reduction in CTB trafficking to the Golgi complex in both WT and Cav1−/− MEFs. In contrast, transferrin (Tf) uptake in cells expressing both Cav1 and the human transferrin receptor (TfR) was not affected by Cav1 expression (unpublished data), suggesting that inhibition is specific for a clathrin-independent pathway.

These results are consistent with previous studies showing that the transient expression of Cav1 reduced endocytosis of several different endocytic markers but extend these studies by showing that short or particularly high expression of Cav1 inhibits CTB uptake. This could reflect an increase in nonendocytic caveolae, which then sequester CTB at the PM into a relatively static domain. This would diminish CTB labeling of the Golgi complex by reducing the amounts of CTB entering the cell. Alternatively, short expression of Cav1 might perturb the cellular lipid balance and so disrupt caveolar and noncaveolar endocytic pathways. This is consistent with findings that expression of Cav1 reduced albumin uptake in HeLa cells but this inhibition was completely reversed and further stimulated by addition of glycosphingolipids (Sharma et al., 2004).

CTB transport to the Golgi occurs via a clathrin- and caveolin-independent pathway that is sensitive to cholesterol depletion

The aforementioned experiments show that caveolae are not required for CTB entry. As CTB internalization has been reported to occur through both clathrin-dependent and -independent pathways (Torgersen et al., 2001; Nichols, 2002; Singh et al., 2003), we examined the contribution of the clathrin coated pit pathway to CTB entry using a well-characterized dominant-negative (DN) form of EPS15 (Benmerah et al., 1999). Expression of EPS15-DN-GFP inhibited Tf uptake in TfR-expressing MEFs by 90% (Fig. 2, G and H). Under these conditions, accumulation of CTB in the Golgi region was only inhibited by 40% (Fig. 2, G and I). Thus, CTB uptake mainly occurred through a noncaveolae nonclathrin pathway.

Next, we examined whether or not the CTB entry pathway in the caveolae-null cells was sensitive to cholesterol depletion. Cyclodextrin treatment was optimized to obtain conditions in which clathrin coated pit–mediated endocytosis was unaffected. As shown in Fig. S3 (available at http://www.jcb.org/cgi/content/full/jcb.200407078/DC1), cyclodextrin treatment for 30 min after a 1-h serum-free period caused a partial block in CTB uptake without affecting Tf uptake. Cholesterol depletion can have diverse effects on cellular function, including disruption of endosomal traffic (Minshall et al., 2000; Le et al., 2002), secretion, (Wang et al., 2000), and even perturbation of the actin network (Kwik et al., 2003). Nevertheless, our results show that cholesterol depletion partially inhibits CTB uptake without affecting Tf uptake.

We examined the role of dynamin in CTB entry. The DN form of dynamin 1, DynK44A, has been shown to inhibit both endogenous dynamin 1 and 2 function and to inhibit clathrin and caveolar endocytosis (Damke et al., 1994; Oh et al., 1998). Therefore, we expressed DynK44A in WT and Cav1−/− MEFs and examined CTB trafficking. As a control, Tf uptake was quantified in the same cells transiently expressing the human TfR. DynK44A reduced Tf uptake by 99–100% (Fig. S4, available at http://www.jcb.org/cgi/content/full/jcb.200407078/DC1). When CTB uptake was examined in Cav1−/− MEFs expressing Dyn1K44A (Fig. 3 A) or Dyn2K44A (not depicted), CTB accumulated in extensive tubular structures (Fig. 3 A) and did not label the Golgi complex after 40 min of internalization (supplementary data). The extent of the tubular network varied from cell to cell. Similar results were obtained with WT MEFs (unpublished data). This network was not labeled by CTB bound to cells at 4°C (Fig. S4), suggesting that the network was intracellular. Therefore, a major fraction of CTB was endocytosed in a dynamin-independent manner into a tubular network induced by the dynamin DN mutant.

To gain further insights into the nonclathrin, noncaveolar endocytic pathway, we examined the effect of an ARF6 mutant on CTB entry. A clathrin-independent ARF6-dependent endocytic route has been described previously (Naslavsky et al., 2004), although recent studies have suggested that CTB entry may occur independently of ARF6 function (Massol et al., 2004). Expression of ARF6 T27N, a DN mutant of ARF6, in

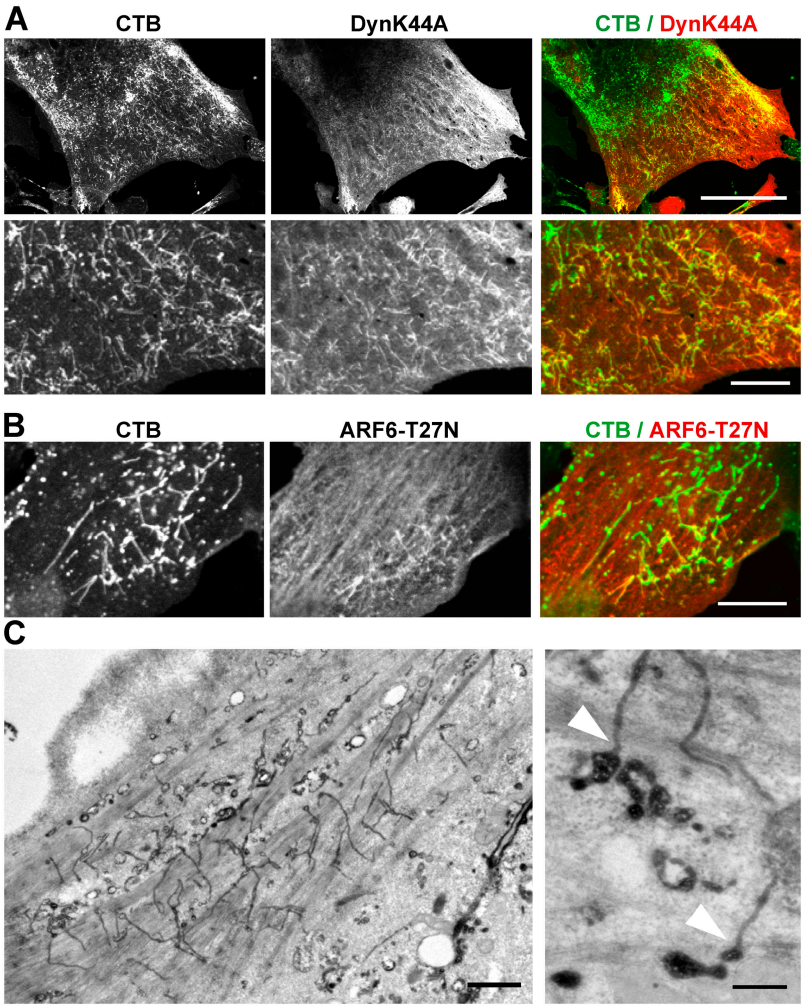

Figure 3. **Dynamin and ARF6 mutants inhibit CTB transport to the Golgi complex.** Cav1−/− MEFs were microinjected with cDNA for DynK44A (A) or ARF6 T27N (B and C; short expression). CTB Alexa Fluor 594 was internalized for 40 min (A and B). DynK44A and ARF6 T27N that contained NH_2-terminal HA tags were labeled with anti-HA (A and B). CTB colocalizes with DynK44A (A) and ARF6 T27N (B) in an extensive tubular network. This is highlighted in enlargements in bottom panels of A. (C) Cav1−/− MEFs were microinjected with ARF6 T27N and HRP, and CTBHRP was internalized for 40 min at 37°C. Cells were prepared for EM and CTBHRP was revealed by DAB cytochemistry. CTBHRP reaction product was evident within a network of 40-nm-diam tubular structures in the injected cells, some of which connect to multivesicular regions (arrowheads). Bars: (A, top; and B) 25 μm; (A, bottom) 5 μm; (C, left) 1 μM; (C, right) 200 nm.

Cav1-null MEFs caused an identical phenotype to the expression of DynK44A (Fig. 3, B and C; and Fig. S5, available at http://www.jcb.org/cgi/content/full/jcb.200407078/DC1). EM of the microinjected cells showed internal CTBHRP-positive tubules attached to multivesicular endosomes. This suggests that CTB uptake occurs through a clathrin-independent, noncaveolar ARF6-independent pathway but suggests that ARF6 mutants disrupt subsequent trafficking to the Golgi complex.

Ultrastructural analysis of CT entry in WT and caveolae-null cells; identification of noncaveolar endocytic carriers

We have shown that CTB internalization does not require caveolae- or clathrin-mediated endocytosis. To characterize the structures involved in CTB uptake, we examined the very first endocytic carriers by EM using the modified DAB/AA method. CTBHRP was bound to Cav1−/− MEFs at 4°C and then the cells were warmed for 15 s to allow visualization of the first internal carriers mediating CTBHRP uptake before fusion with other compartments. The DAB reaction was first performed in the presence of AA to visualize only internal structures, and the cells were not permeabilized before processing. Morphologically distinct CTBHRP-labeled structures could be identified: vesicular structures >70-nm-diam (Fig. 4 A, arrowhead), which were identical to structures labeled with TfHRP at early times of warming (Fig. 4 C), and tubular structures with a tubular profile diameter between 50–80 nm. The latter were the major structures labeled at this time and were often present in groups close to the PM (Fig. 4 A). The tubular structures were often observed as ring-shaped structures (Figs. 4 and 5). In view of the short time of warming, we hypothesized that the tubular/ring-like structures, which were the major structures labeled at this time, were formed through direct budding from the PM. Interestingly, this hypothesis was supported by the observation that similar surface-connected tubular structures could be observed when CTBHRP was bound to the surface of Cav1−/− MEFs and the DAB reaction was performed in the absence of AA (Fig. 4 B). Further markers will be required to confirm that such tubules are indeed the same structures "trapped" at 4°C before budding. An alternative explanation for the formation of the tubular structures could be that short-lived carriers bud from the PM and fuse within 15 s to form tubular endosomes. To examine whether clathrin coated pit–derived vesicles are capable of forming, or fusing with, tubular endosomes, after 15 s in this experimental system, we internalized TfHRP and visualized internal structures. Virtually all TfHRP-

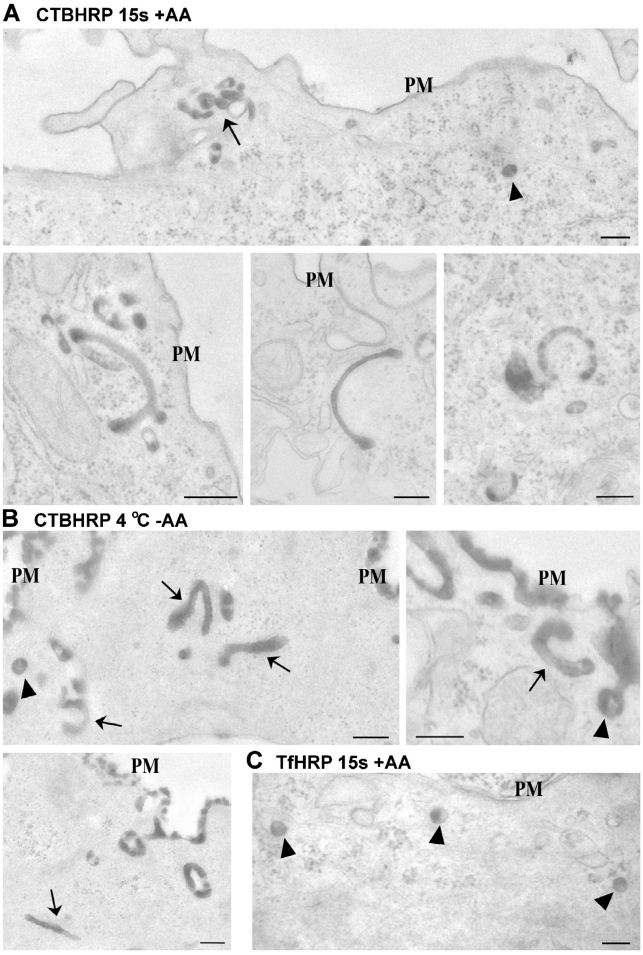

Figure 4. **Ultrastructural characterization of early carriers in Cav1−/− MEFs.** Cav1−/− MEFs were incubated with CTBHRP (A and B) or TfHRP (C) at 4°C. They were warmed for 15 s at 37°C and DAB treated in the presence of AA (A and C) or were DAB treated in the absence of AA without a warming step to reveal the surface distribution of CTBHRP (B). All samples were fixed and processed for EM without permeabilization. (A) CTBHRP reaction product is evident within vesicular profiles (arrowheads) and tubular/ring-shaped profiles (arrows) close to the plasma membrane (PM). Note the groups of labeled structures as most clearly evident in the low magnification overview (top). (B) CTBHRP reaction product is evident over the entire cell surface but tubular/ring-shaped profiles of similar morphology to those detached from the surface after warming are evident (arrows). Also note the labeling of vesicular profiles connected to the cell surface (arrowheads). (C) In contrast to the structures labeled by CTBHRP after 15 s, TfHRP labels vesicular profiles (arrowheads) close to the PM. Bars, 200 nm.

labeled structures (98%; see Materials and methods for details) were vesicular structures of >70-nm-diam rather than tubules (Fig. 4 C). In contrast, 85% of internal CTBHRP-labeled structures showed the tubular/ring-like morphology. The finding that 15% of the structures carrying CTBHRP are derived from the clathrin coated pit pathway supports our functional data on the CTB uptake pathway (Fig. 2). Overall, the data strongly support the hypothesis that the tubular/ring-like structures bud directly from the PM and comprise the first carriers in the nonclathrin, noncaveolae pathway.

To understand the relative importance of each of the early carriers in CTBHRP uptake, the total number of DAB structures within a given area in the periphery of cells was quantified (Fig. 5, E and F). The percentage of CTBHRP-labeled clathrin coated vesicles was the same in WT and Cav1−/− MEFs (Fig. 5 E). When CTBHRP was internalized for 15 s, 1 min, or 5 min, vesicular carriers only made up ~20% of the total DAB-positive structures observed (Fig. 5 E), with the remainder being nonvesicular tubular/ring-shaped carriers in both cell cultures (Fig. 5, A and D). The tubular/ring-like structures were dynamin negative (not depicted), EEA1 negative (not depicted), and in WT MEFs only a minor fraction (5%) were Cav1 positive (Fig. 5, B, C, and F). We conclude that the majority of the early carriers of CTBHRP in both WT and Cav1−/− MEFs were tubular/ring-like structures, as seen in both sectioned (Fig. 5, A and D) and whole-mount specimens (Fig. 5 C and Fig. S1). The whole-mount method revealed the true extent of the tubules in the absence of sectioning and also revealed that the estimate of vesicular carriers in sectioned material, quantified in Fig. 5 E, is likely to be an overestimate due to sectioned tubules appearing as vesicular profiles. However, in WT MEFs, a significant fraction of the internal vesicles of <70 nm are likely to be budded caveolae.

To characterize the tubular/ring-like structures further, we examined whether or not these carriers were sensitive to cholesterol depletion. Using conditions where Tf uptake was unaffected (Fig. S3), WT MEFs were depleted of cholesterol and CTBHRP was internalized for 1 min before the DAB reaction was performed in the presence of AA. In cholesterol-depleted cells, tubular structures only accounted for 35% of the total internal structures compared with 89% in the control cells. This is also an additional confirmation that the tubular carriers are not simply endosomes of the coated pit pathway. This data implies that the tubular carriers are a major component of CTB uptake and are sensitive to cholesterol depletion. We propose that the tubular/ring-like structures bud directly from the PM and are the major carriers involved in the noncaveolae nonclathrin uptake of CTB in both WT and Cav1−/− MEFs. In addition, we speculate that the nonvesicular carriers may be a universal nonclathrin-dependent entry pathway as early noncaveolar CTB-labeled carriers in cell lines, such as Vero cells, NIH3T3, and A431, showed similar morphological characteristics (unpublished data).

Tubular carriers are involved in GPI-AP endocytosis

The structures described here show similarities to the early carriers involved in cdc42-dependent endocytosis of GPI-APs and fluid phase markers (Sabharanjak et al., 2002). Therefore, we incubated WT MEFs with HRP as a fluid phase marker for 15 s. The labeled structures were morphologically similar to the tubular/ring-shaped structures labeled with CTBHRP at early times (Fig. 6 A), consistent with a significant role for these structures in fluid phase uptake. In addition, these results suggest that CTB itself is not dramatically modifying the morphology or formation of the early carriers.

To test directly if a proportion of GPI-APs are cointernalized with CTB, fluorescently-tagged antibodies to GPI-AP, fluorescent-dextran (fluid phase marker), -Tf, and -CTB were cointernalized for 2 min in WT MEFs using the conditions and

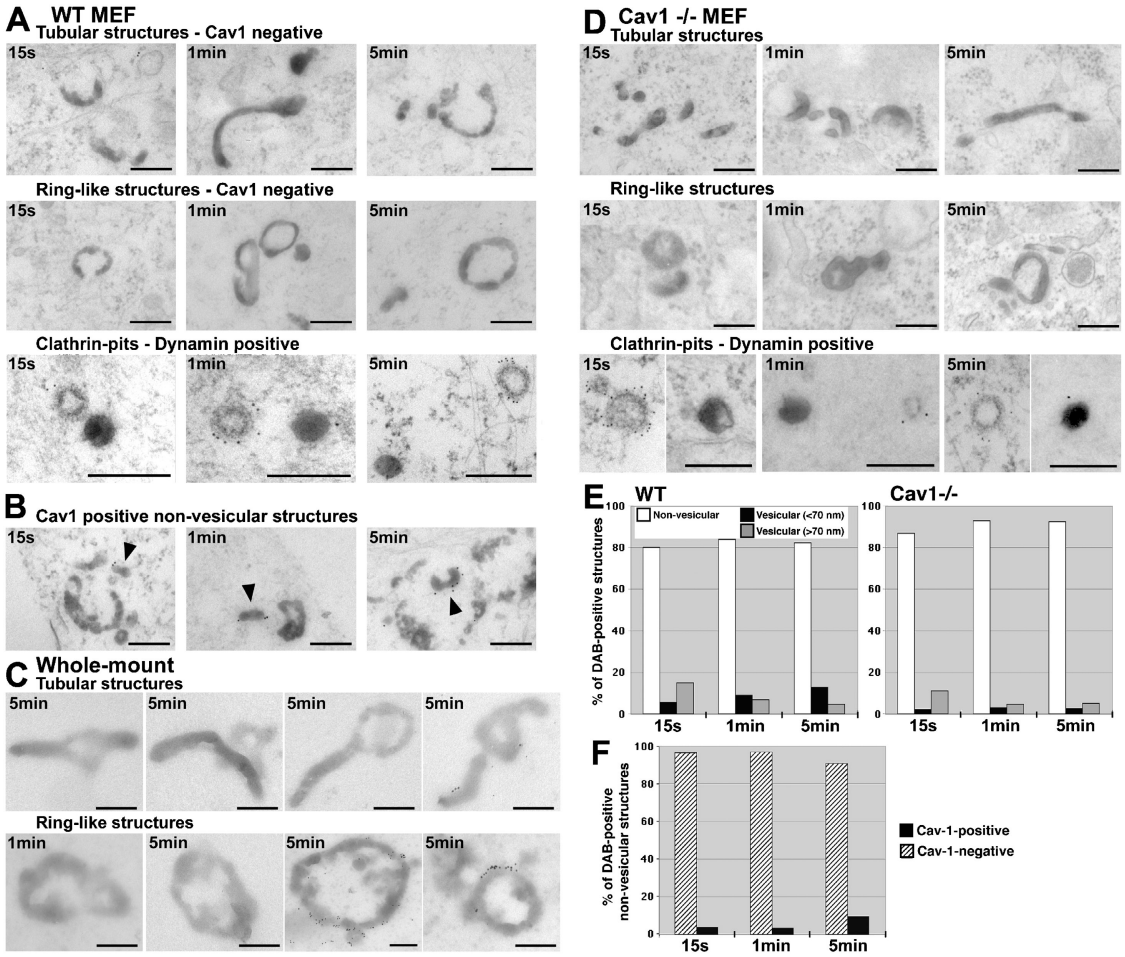

Figure 5. **Ultrastructural characterization of early noncaveolar carriers in Cav1−/− MEFs and WT MEFs.** WT (A, B, and E) and Cav1−/− (D and E) MEFs with bound CTBHRP were warmed for 15 s, 1 min, or 5 min at 37°C and DAB treated in the presence of AA. Samples were immunolabeled for Cav1 (A–C) or dynamin (clathrin-pit panels) and processed for EM. In both WT (A) and Cav1−/− (D) MEFs, CTBHRP reaction product was observed after 15 s, 1 min, and 5 min in tubular structures, ring-like structures, clathrin coated vesicles, and smaller vesicular structures. (B) In WT MEFs, CTBHRP-positive nonvesicular structures partly colocalized with Cav1. The percentage of nonvesicular structures labeled with Cav1 was quantitated (F). (C) WT MEFs were grown on grids, and CTBHRP was internalized for 5 min. Cells were prepared for whole-mount visualization. CTBHRP labeled short tubular or ring-shaped structures, some of which are Cav1 positive. (E) Internal CTBHRP-positive structures in WT and Cav1−/− MEFs were classified according to morphology (see Materials and methods) and quantitated as a percentage of total labeled structures. Most CTBHRP-labeled internal structures in both WT and Cav1−/− MEFs were nonvesicular. Note that visualized structures of <70 nm diam included caveolae. Bars, 200 nm.

reagents of Sabharanjak et al. (2002). In WT MEFs, a pool of endocytosed GPI-APs colocalized with dextran but not Tf (unpublished data), which is consistent with the existence of a noncaveolae nonclathrin pathway for GPI-AP endocytosis and the existence of GPI-AP–enriched early endosomal compartments (GEECs) in these cells as described previously in CHO cells (Sabharanjak et al., 2002). CTB was also observed in dextran-positive but Tf-negative endosomes (Fig. 6, B and C). When GPI-AP, Tf, and CTB were cointernalized, ~70% of all Tf-negative GPI-AP endosomes were labeled with CTB (Fig. 6, D–F). As two Tf ligands of different colors that are cointernalized give a maximum colocalization index of 80% in this assay (Sabharanjak et al., 2002), CTB may mark all GPI-AP internalization through a noncaveolae nonclathrin pathway into GEECs. This implies that the major carriers of the noncaveolae nonclathrin pathway involved in GPI-AP internalization are the tubular/ring-like carriers. In terms of CTB endocytosis, ~50% of total internalized CTB colocalizes with GPI-AP (unpublished data), suggesting that half of the CTB endocytosis occurs via a noncaveolae nonclathrin pathway. This is also consistent with the inability of dynamin and EPS15 inhibitors to completely prevent CTB internalization (Fig. 2, G–I; and Fig. 3 A). Therefore, CTB can be internalized by multiple routes and is not a specific marker for a nonclathrin noncaveolae pathway.

Together, these results strongly suggest that the novel caveolae- and clathrin-independent tubular/ring-like carriers identified here are the same structures, GEECs, shown to be involved in the cdc42-dependent uptake of GPI-APs and fluid phase markers (Sabharanjak et al., 2002). Using the EM methods described here, we are now in a position to undertake a detailed examination of the role of regulatory proteins such as cdc42, which have been implicated in this pathway. Tubular carriers can play a major role in protein transport in other biological membrane systems (Polishchuk et al., 2003) and may

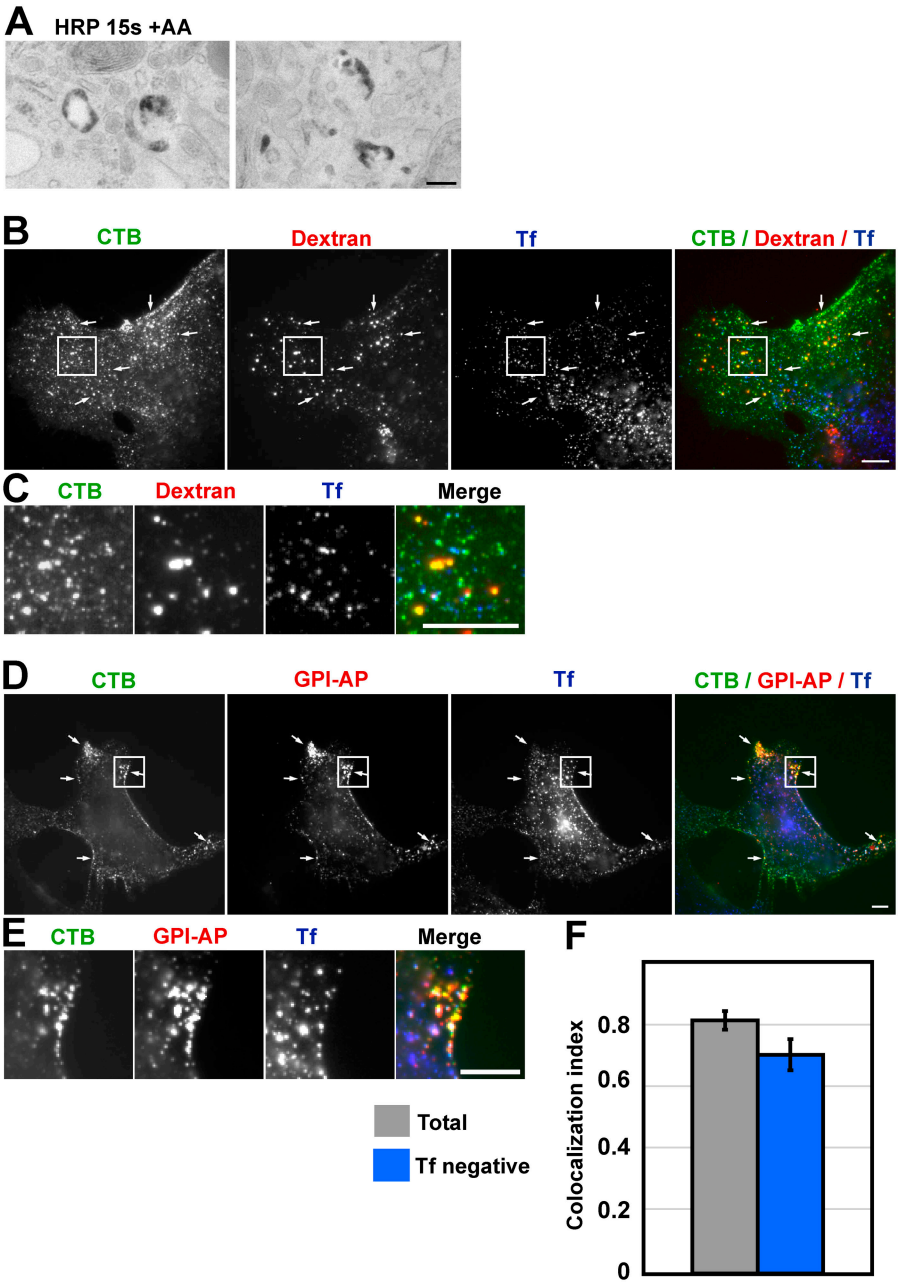

Figure 6. **Analysis of uptake of CTB, fluid phase markers, and GPI-APs.** (A) WT MEFs were incubated with 10 mg/ml HRP as a fluid phase marker for 15 s, and then DAB treated in the presence of AA before being processed for EM. Tubular carriers similar to the early carriers containing CTBHRP are labeled by HRP. (B and C) CTB, dextran, and Tf were cointernalized for 2 min in WT MEFs, and the boxed areas are enlarged in panel C. (D and E) CTB GPI-AP and Tf were cointernalized for 2 min in WT MEFs. CTB colocalization with Tf was observed in ~50% of CTB-positive structures. Arrows highlight endosomes containing CTB and GPI-AP but not Tf, and the boxed areas are enlarged in panel E. (F) GPI-AP and CTB colocalization were quantified to give a colocalization index. Gray bar, colocalization between all GPI-AP–positive structures and CTB; blue bar, CTB colocalization with GPI-AP–positive Tf-negative structures. Error bars indicate standard error. Bars: (A) 200 nm; (B–E) 10 μm.

represent a high capacity system for membrane movement. The ultrastructural characterization of the carriers described here and the development of a method for immunolabeling these structures should facilitate characterization of these carriers in the same way that clathrin coated pit internalization is being elucidated at the molecular level.

Discussion

In this work, we have shown for the first time that bona fide Cav1-positive caveolae can bud from the PM to mediate CTB uptake. Budding can be stimulated by phosphatase inhibitors and by specific lipids. Immunoelectron microscopy quantification of internal Cav1-positive CTBHRP-labeled structures led us to the conclusion that caveolae internalization is a relatively minor pathway in WT MEFs. Previous papers have shown an apparent high level of colocalization of the internalized glycosphingolipid LacCer, CTB, and Cav1 (Singh et al., 2003; Sharma et al., 2004), but this occurred under conditions where LacCer treatment had stimulated caveolae budding (Sharma et al., 2004). We now demonstrate that in the absence of stimulated caveolae budding CTB can be internalized via a noncaveolar pathway, and hence CTB shows low colocalization with Cav1 at the ultrastructural level.

In WT and Cav1−/− MEFs, we have shown that approximately half of the CTB entering the cell is through a clathrin-mediated pathway, but a significant proportion of CTB internalization occurs through a nonclathrin, noncaveolar but cholesterol-sensitive pathway. The precise contribution of each pathway is hard to evaluate using inhibitor studies alone, as

disruption of any one process may cause up-regulation of an alternative pathway (Damke et al., 1995). However, in untreated WT MEFs, a significant proportion of endocytosed CTB colocalizes with GPI-AP and not Tf after short periods of uptake. Moreover, we have also identified and characterized at the ultrastructural level the first structures involved in a major clathrin- and caveolae-independent pathway. These structures are tubular/ring-like with a diameter of 40–80 nm.

It is interesting to speculate that the clathrin-, dynamin-, and caveolin-independent, cholesterol-dependent endocytic pathway described here may, in fact, represent a primitive endocytic mechanism. In budding yeast, endocytosis of fluid phase markers is an actin-based process involving furrowed invaginations of the PM (Mulholland et al., 1999). Endocytosis is affected by specific mutants defective in production of ergosterol, the main sterol of yeast, and can occur without clathrin or dynamin function (Munn, 2001; Pichler and Riezman, 2004). Internalization of both fluid phase markers and GPI-APs in primary cultured cells from *Drosophila melanogaster* is similarly dynamin independent (Guha et al., 2003). Thus, a caveolae- and clathrin-independent pathway may represent a primordial endocytic route. Intriguingly, our studies show that caveolin expression can influence this pathway. This finding raises the possibility that proteins such as caveolin or even clathrin might add an additional level of fine regulatory control of vesicle formation and fission in combination with other proteins of the endocytic machinery such as dynamin.

The involvement of caveolae in endocytosis has been a long-standing question in the field. The upstream receptors that can trigger caveolae budding, perhaps of only a small number of caveolae in vivo, will be of considerable interest. We can also now address whether or not spatially localized subsets of caveolae are internalized in response to specific stimuli. In addition, the morphological characterization of noncaveolar carriers presented here should facilitate more detailed studies of a specialized endocytic pathway for which the molecular machinery and cellular functions are currently largely unknown.

Materials and methods

Antibodies and reagents

Expression plasmids were generated or obtained from the following sources: pIRES2-EGFP/Cav1 (gift of C.J. Fielding, University of California, San Francisco, San Francisco, CA), TfR (gift of V. Gerke, Center for Molecular Biology of Inflammation (ZMBE), University of Muenster, Muenster, Germany), pEGFP-EPS-15/EΔ95/295 (gift of A. Yap, University of Queensland, Queensland, Australia), pCB DYN-K44A-HA (gift by S.L. Schmid, Scripps Research Institute, La Jolla, CA), and pXS/HA-ARF-6 T27N (gift of J.L Donaldson, Laboratory of Cell Biology, National Heart, Lung, and Blood Institute, National Institutes of Health, Bethesda, MD). Antibodies were obtained from the following sources: rabbit anti-caveolin and mouse anti-GM130 (BD Biosciences), rabbit anti-CT (Sigma-Aldrich), rabbit anti-HA (provided by T. Nilsson, Gothenburg University, Gothenburg, Sweden), and mouse anti-dynamin, Hudy1 (S.L. Schmid). Secondary antibodies conjugated to Alexa Fluor 488, 647, or 660 and CTB conjugated to Alexa Fluor 594 and Tf -Alexa Fluor 546 (Molecular Probes) were used. All other reagents were purchased from Sigma-Aldrich unless otherwise stated.

Cell culture and microinjection

MEFs were generated from 13.5-d-old embryos from either pregnant Cav1−/− mice or litter-matched WT mice as described previously (Razani et al., 2001). MEF cells were cultured in DME supplemented with 10% FCS, 2 mM L-glutamine, 100 U/ml penicillin, and 100 μg/ml streptomycin (Invitrogen). MEF cells were not immortalized, and thus cells were only cultured to passage 6. Microinjection was performed as described previously (Richards et al., 2002). Cells were injected in the nucleus with 50–100 μg/ml of plasmid DNA and allowed to recover overnight in normal growth media at 37°C. For short expression of proteins, cells were injected with 150–200 μg/ml of plasmid DNA and allowed to recover for 5–6 h before subsequent manipulations.

Immunofluorescence and cell labeling

Cells were processed for immunofluorescence microscopy as described previously (Richards et al., 2002). CTB uptake was performed essentially as described previously (Sotgia et al., 2002). In brief, 0.05–1 μg/ml CTB was bound to the cells on ice for 30 min in CO_2-independent medium (GIBCO BRL) containing 2 mM L-glutamine and washed on ice in CO_2-independent medium before internalization at 37°C, 5% CO_2 in prewarmed normal growth media, for various times. Tf internalization was performed by first incubating the cells for 1 h in DME and 2 mM L-glutamine, and then placing the cells in prewarmed DME with 10 μg/ml Tf, normal growth media for 20 min at 37°C, unless otherwise stated. The cells were washed on ice in CO_2-independent medium/acetic acid, pH 4.0, for 4 min followed by a 5-min wash in CO_2-independent medium. Cholesterol depletion of the cells was performed by treating the cells for 1 h in DME and L-glutamine and then incubating in DME containing 10 mg/ml methyl-β-cyclodextrin for 30 min at 37°C, 5% CO_2. Any subsequent uptake experiments were performed in DME containing 10% (vol/vol) Lipoprotein-depleted serum. 25 μM LacCer and 1 μM OA treatment were prepared and performed as described previously (Parton et al., 1994; Sharma et al., 2004).

An assay based on cAMP-dependent cell morphology change was used to assess CT-induced toxicity as described previously (Massol et al., 2004). Cells were incubated with cholera holotoxin (Sigma-Aldrich) in DME plus 0.5% BSA for 2 h before the samples were scored for a change in cell morphology. Brefeldin A (5 μg/ml) treatment was performed on cells for 1 h in normal growth media before incubation with CT in the continued presence of brefeldin A. Experiments were repeated three times.

Microscopy and fluorescence quantification

All images were taken on a 1024 confocal system using Lasersharp 2000 4.0. software (Bio-Rad Laboratories), Plan APO 60× (Olympus), NA 1.4, 20 W Kr:Ar laser or on a radiance 2000 confocal system (Bio-Rad Laboratories) using Lasersharp 2000 4.0. software, Plan APO 100× (Nikon), NA 1.4, 50 W Ar laser (488 nm excitation), He:Ne (543 nm excitation) Red Diode (638 nm excitation; Fig. 3, A and B). Fig. 3 B was imaged using 3× digital zoom. All images were acquired at RT and all fluorochromes used are described in Antibodies and reagents. All images were processed using Adobe Photoshop version 7.0 and figures compiled with Adobe Illustrator version 10.0. Cells prepared for immunofluorescence microscopy were mounted in 0.4% (wt/vol) p-phenylenediame, 85% glycerol, and 20 mM Tris, pH 9.

CTB and Tf uptake was quantified on samples prepared simultaneously using identical conditions. Images used for quantification were taken through the center of the cell as judged by maximizing Golgi labeling (GM130) or Tf. All images were taken with identical acquisition parameters per experiment, and then individual cells were cut out using Adobe Photoshop version 7.0. To quantify CTB accumulation in the Golgi and Tf uptake, a mask-overlay method was used (see Online supplemental material).

Ultrastructural immunogold analysis of CTBHRP, TfHRP, and HRP uptake

MEF cells, cultured on 3-cm dishes, were washed in CO_2-independent medium, incubated in CO_2-independent medium containing 10 μg/ml CTB-HRP at 4°C for 20 min, and then CTBHRP was internalized at 37°C in normal growth media. To stop internalization, the cells were placed on ice in pre-chilled CO_2-independent medium. Next, the cells were incubated for 20 min at 4°C in freshly prepared DAB buffer (1 mg/ml DAB and 0.012% H_2O_2) with or without 50 mM AA in PBS and fixed with 2.5% glutaraldehyde for 1 h. MEFs were incubated with DME plus L-glutamine for 1 h at 37°C before being incubated with 30 μg/ml TfHRP at 4°C for 20 min in CO_2-independent medium. This was followed by 15 s uptake in normal growth media. The cells were processed for EM as described for CTHRP. Fluid phase marker HRP (10 mg/ml) was continuously internalized in normal growth media for 15 s, cells were washed in PBS and incubated in DAB buffer in the presence of AA for 5 min at RT before fixation with 2.5% glutaraldehyde for 1 h. Cells were embedded in Epon and cut parallel to the culture substratum.

For immunolabeling, cells were fixed in 4% PFA at RT for 1 h. They were then incubated sequentially with 20 mM glycine in PBS (10 min),

blocking solution (2% BSA in PBS, 10 min), and 0.1% Triton X-100 in PBS (10 min). The cells were incubated with the blocking solution containing the primary antibodies for 2 h, washed in PBS, then incubated anti–mouse or rabbit IgG gold (5 or 10 nm) in blocking solution for 2 h. Cells were washed in PBS and fixed in 2.5% glutaraldehyde for 1 h to permanently immobilize the colloidal gold labeling. The cells were embedded in Epon and cut parallel to the culture substratum. Additional "on-grid" staining of sectioned material with uranyl acetate and lead citrate was performed when required.

Preparation of whole-mount specimens

Whole-mount cells were prepared by a modification of the protocol described previously (Stoorvogel et al., 1996). MEFs were grown for 24–30 h on golden grids (ProSciTech) carrying a carbon-coated Formvar film. After internalization of CTBHRP, DAB reactions were performed in the presence of AA. Cells were permeabilized with 0.1% Triton X-100 for 30 min before fixation with 1% PFA for 1 h at 4°C and immunolabeled as described in the previous paragraph. After final fixation with 2.5% glutaraldehyde, the cells were extensively washed with H_2O and the grids were immersed in methylcellulose for 5 min, allowed to dry, and viewed without further processing.

Quantification of EM

To determine the percentage of internalized CTBHRP-positive endosomal and vesicular structures, all DAB-positive structures were counted in a given peripheral region of a cell in thin sections. Labeled structures were classified as follows (Figs. 1, 4, and 5): nonvesicular structures, DAB-positive tubular and ring-like structures; vesicular structures, DAB-positive round profiles of either 50–70 nm or >70 nm diameter. Caveolae were defined by their characteristic size (50–70 nm diameter), shape, and Cav1 labeling. To determine the percentage of total caveolae that were intracellular, extracellular HRP reactions were inhibited by AA, and DAB-positive and -negative caveolae were counted. In both cases, random fields were photographed at a primary magnification of 30 K. Approximately 40–50 micrographs were examined for each condition.

To quantitate the effect of cholesterol depletion on CTBHRP internalization and to quantitatively compare the carriers involved in uptake of Tf and CTBHRP at early times, DAB-positive structures were classified as vesicular (>70 nm structures of vesicular appearance) or tubular (Figs. 4 and 5) in fields selected at random. Approximately 100–400 labeled structures were examined, and similar results were obtained in two independent experiments.

GPI-AP internalization and quantification

GPI-AP internalization experiments were performed as described previously (Sabharanjak et al., 2002) using WT MEFs. In brief, mCFP-GPI was transiently expressed by transfection using Fugene (Roche) or microinjection of plasmid DNA. FAB fragment of anti-GFP-antibody coupled to 4 μg/ml CY3, 1 μg/ml Alexa Fluor 488 CTB, 40 μg/ml Alexa Fluor 647 Tf, or 1 mg/ml TMR dextran were cointernalized in various combinations for 2 min. After endocytosis, cells were treated with AA buffer, PI-PLC, and isotonic Glycine-HCl buffer, pH 1.5, to remove surface bound Tf, CFP-GPI, and CTB, respectively. Cells were fixed and processed for high resolution wide-field microscopy. All imaging and quantification methods used to determine endocytic marker overlap were identical to those previously described (Sabharanjak et al., 2002).

Online supplemental material

Fig. S1 shows the development and validation of the technique for ultrastructural analysis of the early endocytic carriers in MEFs. Fig. S2 shows de novo formation of caveolae upon expression of Cav1 in Cav1−/− MEFs. Fig. S3 demonstrates that CTB uptake in Cav1−/− MEFs is partly sensitive to cholesterol depletion. Figs. S4 and S5 show that mutants of both dynamin and ARF6 inhibit CTB transport to the Golgi complex but not internalization. Supplemental Materials and methods contain additional information regarding the quantification of CTB accumulation within a GM130-positive region and the quantification of Tf uptake. Online supplemental material is available at http://www.jcb.org/cgi/content/full/jcb.200407078/DC1.

We thank Charles Ferguson for help with EM.

This study was supported by a Program Grant from the National Health and Medical Research Council of Australia to R.G. Parton and J.F. Hancock. The Centre for Functional and Applied Genomics is a Special Research Center of the Australian Research Council.

Submitted: 13 July 2004
Accepted: 23 November 2004

References

Anderson, R.G., B.A. Kamen, K.G. Rothberg, and S.W. Lacey. 1992. Potocytosis: sequestration and transport of small molecules by caveolae. *Science.* 255:410–411.

Benmerah, A., M. Bayrou, N. Cerf-Bensussan, and A. Dautry-Varsat. 1999. Inhibition of clathrin coated pit assembly by an Eps15 mutant. *J. Cell Sci.* 112:1303–1311.

Conner, S.D., and S.L. Schmid. 2003. Regulated portals of entry into the cell. *Nature.* 422:37–44.

Damke, H., T. Baba, D.E. Warnock, and S.L. Schmid. 1994. Induction of mutant dynamin specifically blocks endocytic coated vesicle formation. *J. Cell Biol.* 127:915–934.

Damke, H., T. Baba, A.M. van der Bliek, and S.L. Schmid. 1995. Clathrin-independent pinocytosis is induced in cells overexpressing a temperature-sensitive mutant of dynamin. *J. Cell Biol.* 131:69–80.

Guha, A., V. Sriram, K.S. Krishnan, and S. Mayor. 2003. Shibire mutations reveal distinct dynamin-independent and -dependent endocytic pathways in primary cultures of *Drosophila* hemocytes. *J. Cell Sci.* 116:3373–3386.

Kaisto, T., P. Rahkila, V. Marjomaki, R.G. Parton, and K. Metsikko. 1999. Endocytosis in skeletal muscle fibers. *Exp. Cell Res.* 253:551–560.

Kwik, J., S. Boyle, D. Fooksman, L. Margolis, M.P. Sheetz, and M. Edidin. 2003. Membrane cholesterol, lateral mobility, and the phosphatidylinositol 4,5-bisphosphate-dependent organization of cell actin. *Proc. Natl. Acad. Sci. USA.* 100:13964–13969.

Lamaze, C., A. Dujeancourt, T. Baba, C.G. Lo, A. Benmerah, and A. Dautry-Varsat. 2001. Interleukin 2 receptors and detergent-resistant membrane domains define a clathrin-independent endocytic pathway. *Mol. Cell.* 7:661–671.

Le, P.U., G. Guay, Y. Altschuler, and I.R. Nabi. 2002. Caveolin-1 is a negative regulator of caveolae-mediated endocytosis to the endoplasmic reticulum. *J. Biol. Chem.* 277:3371–3379.

Massol, R.H., J.E. Larsen, Y. Fujinaga, W.I. Lencer, and T. Kirchhausen. 2004. Cholera toxin toxicity does not require functional Arf6- and dynamin-dependent endocytic pathways. *Mol. Biol. Cell.* 15:3631–3641.

Minshall, R.D., C. Tiruppathi, S.M. Vogel, W.D. Niles, A. Gilchrist, H.E. Hamm, and A.B. Malik. 2000. Endothelial cell-surface gp60 activates vesicle formation and trafficking via G_i-coupled *Src* kinase signaling pathway. *J. Cell Biol.* 150:1057–1070.

Mulholland, J., J. Konopka, B. Singer-Kruger, M. Zerial, and D. Botstein. 1999. Visualization of receptor-mediated endocytosis in yeast. *Mol. Biol. Cell.* 10:799–817.

Munn, A.L. 2001. Molecular requirements for the internalisation step of endocytosis: insights from yeast. *Biochim. Biophys. Acta.* 1535:236–257.

Naslavsky, N., R. Weigert, and J.G. Donaldson. 2004. Characterization of a nonclathrin endocytic pathway: membrane cargo and lipid requirements. *Mol. Biol. Cell.* 15:3542–3552.

Nichols, B.J. 2002. A distinct class of endosome mediates clathrin-independent endocytosis to the Golgi complex. *Nat. Cell Biol.* 4:374–378.

Oh, P., D.P. McIntosh, and J.E. Schnitzer. 1998. Dynamin at the neck of caveolae mediates their budding to form transport vesicles by GTP-driven fission from the plasma membrane of endothelium. *J. Cell Biol.* 141:101–114.

Orlandi, P.A., and P.H. Fishman. 1998. Filipin-dependent inhibition of cholera toxin: evidence for toxin internalization and activation through caveolae-like domains. *J. Cell Biol.* 141:905–915.

Pang, H., P.U. Le, and I.R. Nabi. 2004. Ganglioside GM1 levels are a determinant of the extent of caveolae/raft-dependent endocytosis of cholera toxin to the Golgi apparatus. *J. Cell Sci.* 117:1421–1430.

Parton, R.G. 1994. Ultrastructural localization of gangliosides; GM1 is concentrated in caveolae. *J. Histochem. Cytochem.* 42:155–166.

Parton, R.G., and A.A. Richards. 2003. Lipid rafts and caveolae as portals for endocytosis: new insights and common mechanisms. *Traffic.* 4:724–738.

Parton, R.G., B. Joggerst, and K. Simons. 1994. Regulated internalization of caveolae. *J. Cell Biol.* 127:1199–1215.

Parton, R.G., J.C. Molero, M. Floetenmeyer, K.M. Green, and D.E. James. 2002. Characterization of a distinct plasma membrane macrodomain in differentiated adipocytes. *J. Biol. Chem.* 277:46769–46778.

Pelkmans, L., J. Kartenbeck, and A. Helenius. 2001. Caveolar endocytosis of simian virus 40 reveals a new two-step vesicular-transport pathway to the ER. *Nat. Cell Biol.* 3:473–483.

Pelkmans, L., D. Puntener, and A. Helenius. 2002. Local actin polymerization and dynamin recruitment in SV40-induced internalization of caveolae. *Science.* 296:535–539.

Pichler, H., and H. Riezman. 2004. Where sterols are required for endocytosis. *Biochim. Biophys. Acta.* 1666:51–61.

Polishchuk, E.V., A. Di Pentima, A. Luini, and R.S. Polishchuk. 2003. Mechanism of constitutive export from the golgi: bulk flow via the formation, protrusion, and en bloc cleavage of large trans-golgi network tubular domains. *Mol. Biol. Cell.* 14:4470–4485.

Razani, B., J.A. Engelman, X.B. Wang, W. Schubert, X.L. Zhang, C.B. Marks, F. Macaluso, R.G. Russell, M. Li, R.G. Pestell, et al. 2001. Caveolin-1 null mice are viable but show evidence of hyperproliferative and vascular abnormalities. *J. Biol. Chem.* 276:38121–38138.

Richards, A.A., E. Stang, R. Pepperkok, and R.G. Parton. 2002. Inhibitors of COP-mediated transport and cholera toxin action inhibit simian virus 40 infection. *Mol. Biol. Cell.* 13:1750–1764.

Sabharanjak, S., P. Sharma, R.G. Parton, and S. Mayor. 2002. GPI-anchored proteins are delivered to recycling endosomes via a distinct cdc42-regulated, clathrin-independent pinocytic pathway. *Dev. Cell.* 2:411–423.

Severs, N.J. 1988. Caveolae: static inpocketings of the plasma membrane, dynamic vesicles or plain artifact? *J. Cell Sci.* 90:341–348.

Shajahan, A.N., B.K. Timblin, R. Sandoval, C. Tiruppathi, A.B. Malik, and R.D. Minshall. 2004. Role of Src-induced dynamin-2 phosphorylation in caveolae-mediated endocytosis in endothelial cells. *J. Biol. Chem.* 279:20392–20400.

Sharma, D.K., J.C. Brown, A. Choudhury, T.E. Peterson, E. Holicky, D.L. Marks, R. Simari, R.G. Parton, and R.E. Pagano. 2004. Selective stimulation of caveolar endocytosis by glycosphingolipids and cholesterol. *Mol. Biol. Cell.* 15:3114–3122.

Shogomori, H., and A.H. Futerman. 2001. Cholera toxin is found in detergent-insoluble rafts/domains at the cell surface of hippocampal neurons but is internalized via a raft-independent mechanism. *J. Biol. Chem.* 276:9182–9188.

Singh, R.D., V. Puri, J.T. Valiyaveettil, D.L. Marks, R. Bittman, and R.E. Pagano. 2003. Selective caveolin-1-dependent endocytosis of glycosphingolipids. *Mol. Biol. Cell.* 14:3254–3265.

Sotgia, F., B. Razani, G. Bonuccelli, W. Schubert, M. Battista, H. Lee, F. Capozza, A.L. Schubert, C. Minetti, J.T. Buckley, and M.P. Lisanti. 2002. Intracellular retention of glycosylphosphatidyl inositol-linked proteins in caveolin-deficient cells. *Mol. Cell. Biol.* 22:3905–3926.

Souto, R.P., G. Vallega, J. Wharton, J. Vinten, J. Tranum-Jensen, and P.F. Pilch. 2003. Immunopurification and characterization of rat adipocyte caveolae suggest their dissociation from insulin signaling. *J. Biol. Chem.* 278:18321–18329.

Stang, E., J. Kartenbeck, and R.G. Parton. 1997. Major histocompatibility complex class I molecules mediate association of SV40 with caveolae. *Mol. Biol. Cell.* 8:47–57.

Stoorvogel, W., V. Oorschot, and H.J. Geuze. 1996. A novel class of clathrin coated vesicles budding from endosomes. *J. Cell Biol.* 132:21–33.

Thomsen, P., K. Roepstorff, M. Stahlhut, and B. van Deurs. 2002. Caveolae are highly immobile plasma membrane microdomains, which are not involved in constitutive endocytic trafficking. *Mol. Biol. Cell.* 13:238–250.

Torgersen, M.L., G. Skretting, B. van Deurs, and K. Sandvig. 2001. Internalization of cholera toxin by different endocytic mechanisms. *J. Cell Sci.* 114:3737–3747.

Tsai, B., J.M. Gilbert, T. Stehle, W. Lencer, T.L. Benjamin, and T.A. Rapoport. 2003. Gangliosides are receptors for murine polyoma virus and SV40. *EMBO J.* 22:4346–4355.

van Deurs, B., K. Roepstorff, A.M. Hommelgaard, and K. Sandvig. 2003. Caveolae: anchored, multifunctional platforms in the lipid ocean. *Trends Cell Biol.* 13:92–100.

Wang, Y., C. Thiele, and W.B. Huttner. 2000. Cholesterol is required for the formation of regulated and constitutive secretory vesicles from the trans-Golgi network. *Traffic.* 1:952–962.

Wolf, A.A., M.G. Jobling, S. Wimer-Mackin, M. Ferguson-Maltzman, J.L. Madara, R.K. Holmes, and W.I. Lencer. 1998. Ganglioside structure dictates signal transduction by cholera toxin and association with caveolae-like membrane domains in polarized epithelia. *J. Cell Biol.* 141:917–927.